



OPEN

Thermoelectricity in atom-sized junctions at room temperatures

SUBJECT AREAS:

MOLECULAR
ELECTRONICS

NEMS

QUANTUM MECHANICS

NANOSENSORS

Makusu Tsutsui, Takanori Morikawa, Akihide Arima & Masateru Taniguchi

The Institute of Scientific and Industrial Research, Osaka University, 8-1 Mihogaoka, Ibaraki, Osaka 567-0047, Japan.

Atomic and molecular junctions are an emerging class of thermoelectric materials that exploit quantum confinement effects to obtain an enhanced figure of merit. An important feature in such nanoscale systems is that the electron and heat transport become highly sensitive to the atomic configurations. Here we report the characterization of geometry-sensitive thermoelectricity in atom-sized junctions at room temperatures. We measured the electrical conductance and thermoelectric power of gold nanocontacts simultaneously down to the single atom size. We found junction conductance dependent thermoelectric voltage oscillations with period $2e^2/h$. We also observed quantum suppression of thermovoltage fluctuations in fully-transparent contacts. These quantum confinement effects appeared only statistically due to the geometry-sensitive nature of thermoelectricity in the atom-sized junctions. The present method can be applied to various nanomaterials including single-molecules or nanoparticles and thus may be used as a useful platform for developing low-dimensional thermoelectric building blocks.

Received

21 August 2013

Accepted

8 November 2013

Published

25 November 2013

Correspondence and requests for materials should be addressed to M.T. (tsutsui@sanken.osaka-u.ac.jp)

A temperature gradient in a material induces diffusion of majority charge carriers from the hot to the cold region and builds electric voltage there. This thermoelectric effect enables direct conversion of thermal energy into electricity or vice versa without need of mechanical components; an ideal route for power generation being a silent and greenhouse gas emission-free technology. A fundamental issue in thermoelectric generators has been the low efficiency of the constituent materials, which are required to possess conflicting properties of low thermal conductivity and electrical resistivity in addition to high thermopower^{1,2}. This so-called phonon-glass electron-crystal concept has led to significant improvements of the thermoelectric figure of merit in bulk materials though yet to reach an acceptable level for the practical applications¹⁻⁴.

An emerging approach for high-performance thermoelectric materials is to exploit quantum effects in low-dimensional nanostructures that provides high electronic density of states for enhanced Seebeck coefficients^{5,6}. Thermoelectric transport in atomic and molecular junctions, confined systems with discrete states, has recently been studied intensively in this respect⁷⁻¹³. Significant enhancement of thermopower was reported in Bi quantum point contacts attaining several mV/K¹⁰. Positive and negative thermovoltage was also found in metal-molecule-metal bridges in where current was carried through the highest occupied and lowest unoccupied molecular orbitals, respectively; a key finding in constructing thermoelectric devices with molecular junctions¹¹. Despite the progress, however, little experimental efforts have been devoted to elucidate the high sensitivity of thermoelectric power on the atomic junction configurations; an essential feature that needs to be understood and controlled for tailoring the unique properties in such quantum systems¹²⁻¹⁴.

Here we describe a method for evaluating the geometrical dependence of thermopower in nanoscale conductors. We developed a microheater-embedded mechanically-controllable break junction (MCBJ). It combines the ability to control the local temperature at the microfabricated electrical resistance Pt heater¹⁵ with the MCBJ technique for repeatedly forming stable atomic and molecular junctions of varying configurations¹⁶ (Fig. 1a–b; fabrication procedures are available in Methods section and Supplementary Information Fig. S1). We imposed a temperature gradient by applying a dc voltage V_b to the Pt heater and performed simultaneous measurements of the electrical conductance G and the thermoelectric voltage ΔV of Au atom-sized constrictions repeatedly at room temperatures in a vacuum (Fig. 1a–b; see also Fig. S1).

Results

Slowly stretching a Au nanocontact, G measured at the applied voltage $V_b = 0.1$ V decreased to zero in a stepwise manner reflecting atom rearrangements during elastic/plastic deformations that cause discontinuous changes in the cross-sectional area at a nanoconstriction (Fig. 1d)¹⁷. When a contact is narrowed and becomes comparable to the Fermi wavelength λ_F , which is about 0.5 nm, we enter into a full quantum limit wherein G complies with

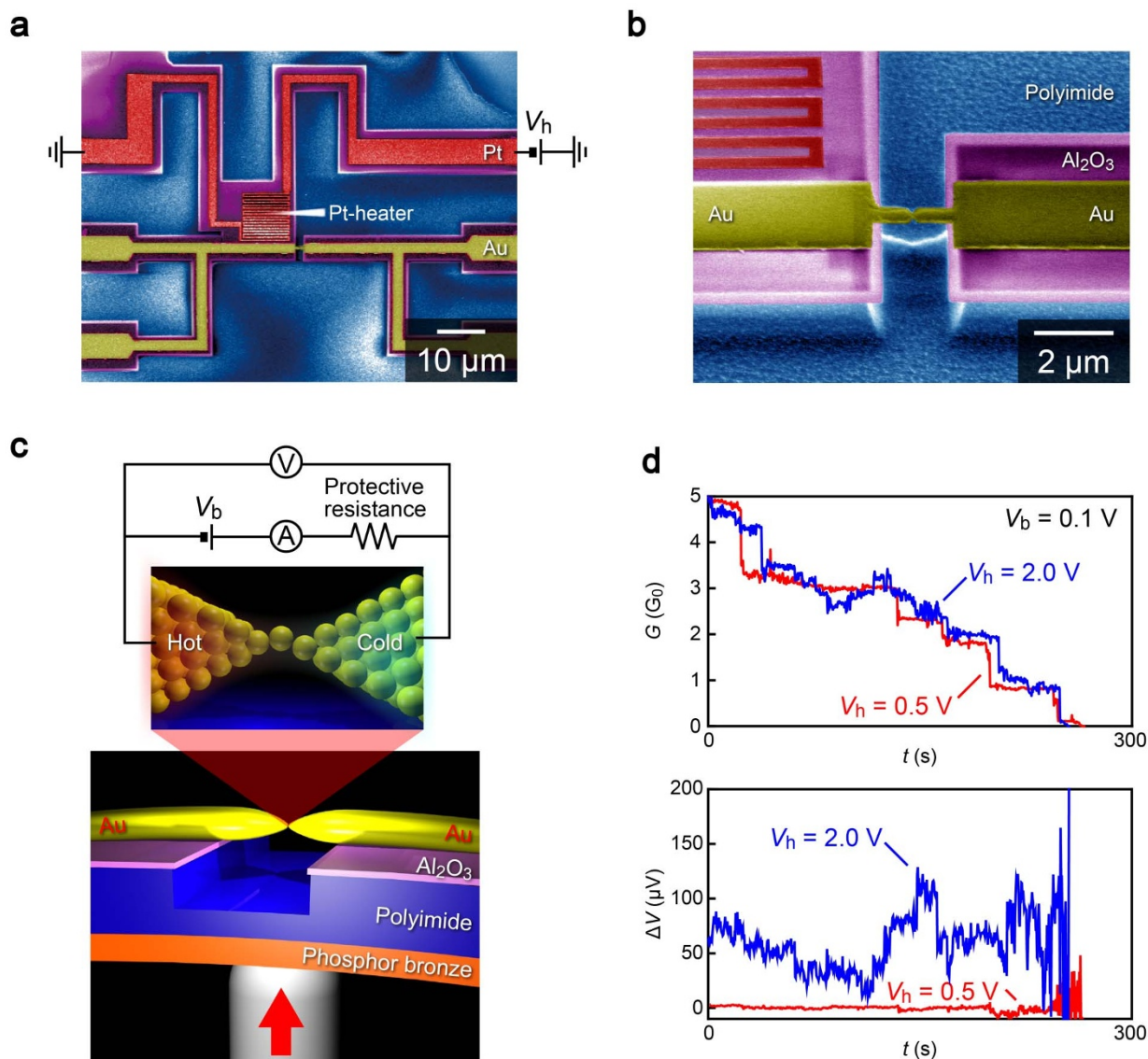


Figure 1 | Simultaneous measurements of single-atom conductance and thermoelectric voltage. (a–b), Scanning electron micrographs of a heater-embedded mechanically-controllable break junction. It consists of a Au nanobridge and a Pt microheater fabricated on thin Al_2O_3 layers patterned on a polyimide-coated phosphor-bronze substrate. A temperature gradient was created at the junction by electrically heating the Pt heater through applying a dc voltage V_h . (c), Au single-atom contacts were formed by exerting tensile forces on the junctions through controlling a deflection of the substrate via a piezo-control. Concurrent recording of the junction conductance G and the thermoelectric voltage ΔV were conducted under constant V_h . The voltage source was switched off upon measuring ΔV . (d), Time traces of G and ΔV during stretching of a Au nanocontact at room temperatures in a vacuum under $V_h = 0.5$ V and 2.0 V. Conductance decreased in a stepwise fashion and exhibited a plateau at one unit of conductance quantum signifying formation of Au single-atom chains. Meanwhile, ΔV showed large fluctuations ascribed to a change in the electronic structure.

Landauer formula $\sum_i T_i G_0$ ($i = 1, 2, 3 \dots n$)¹⁸. Here, T_i is the transmission coefficient in the i th channel and $G_0 = 2e^2/h$ is the conductance quantum. Plateaus appeared at near $1 G_0$ signify formation of Au single-atom chains with a fully-open channel for charge transmission^{17,19}. The staircase-like structure was observed in all the $G - t$ traces acquired in a range of V_h from 0 to 3 V. In contrast, the thermoelectric voltage simultaneously recorded with G responded sharply to the V_h conditions: ΔV is several μV at $V_h = 0.5$ V but increases by an order of magnitude at $V_h = 2.0$ V (Fig. 1d; background voltage has been subtracted using the data obtained at $V_h = 0$ V as explained in Supplementary Information Figs. S2 and S3). Furthermore, ΔV fluctuated substantially upon mechanical elongation in the course of tensile loading manifesting geometry-sensitive thermoelectricity in atom-sized junctions (Figs. S4 and S5).

Statistical distributions of G and ΔV were explored to investigate thermoelectric transport in ballistic Au nanocontacts. Conductance

histograms constructed with 50 $G-t$ curves exhibit peaks at integer multiples of $2e^2/h$ with slight deviations attributable to the virtual series resistance R_s of 800Ω associated with defect scattering in the electron reservoirs (Fig. 2a)^{17,20}. The low-conductance feature in the histogram below $1 G_0$ suggests adsorption of gas molecules on the junction surface that affects the conductance of Au single-atom contacts^{21,22}. On the other hand, ΔV exhibits single-peak distributions (Fig. 2b inset). Here, the center of the peak, ΔV_p , represents the thermoelectric voltage generated at relatively large junctions having G of 5 to 8 G_0 . The plots reveal monotonic increase of ΔV_p with V_h^2 (blue line in Fig. 2b), which manifests that one side of the Au nanocontact has been heated to an elevated temperature via the Joule heat dissipated at the current-carrying Pt coil (Supplementary Information Fig. S6).

To reveal any quantum confinement effects in thermoelectricity in Au nanocontacts at a single-atom level, we deduced the average

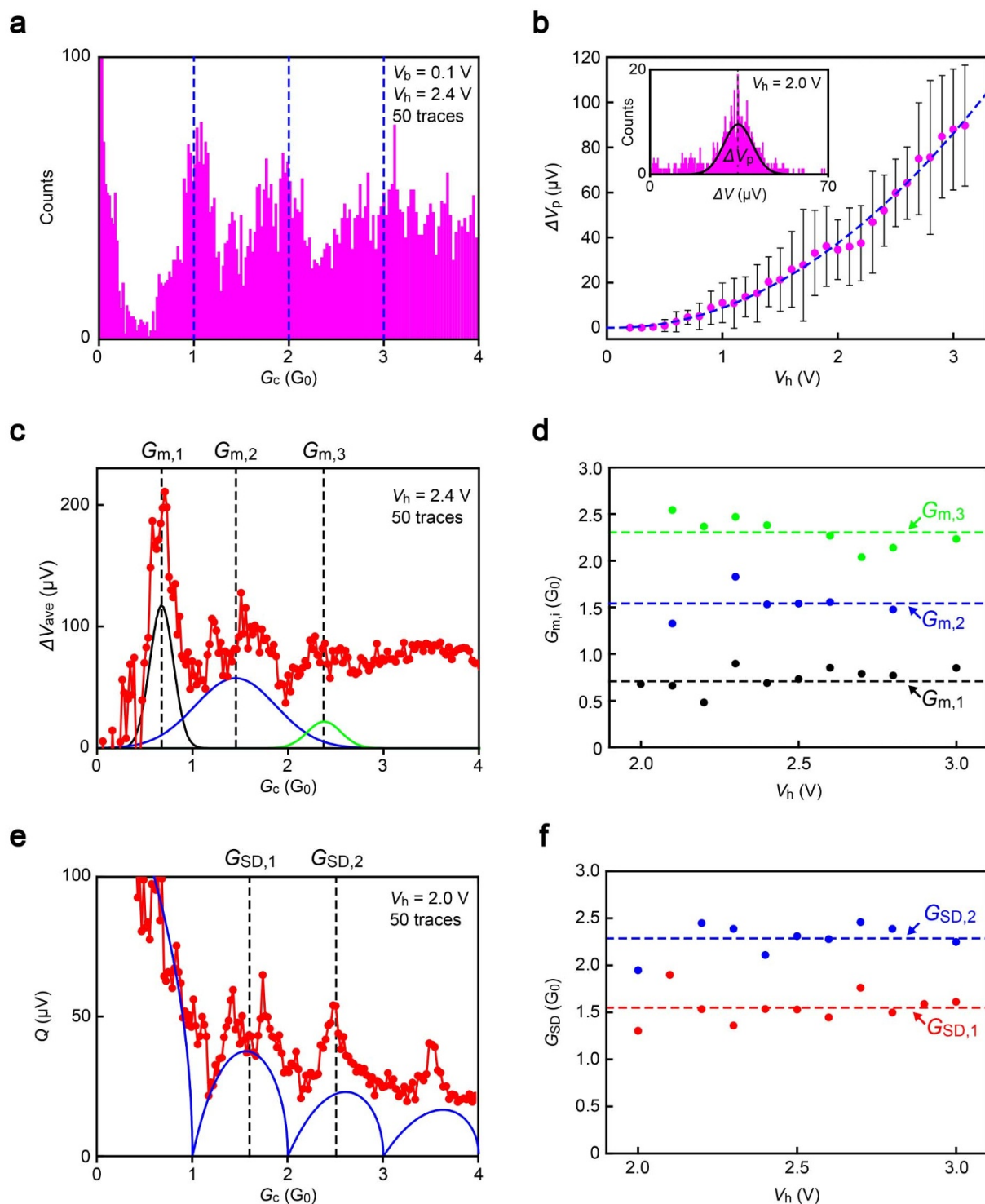


Figure 2 | Quantized thermoelectric voltage in ballistic Au atom-sized contacts. (a), Conductance histogram showing peaks at multiple integer of $2e^2/h$. Dotted lines mark the expected quantized conductance states with a virtual serial resistance R_s of 800Ω . (b), Plots of the thermoelectric voltage of Au nanocontacts ΔV_p extracted by Gaussian fitting to the ΔV distributions (inset) as a function of the voltage applied to the Pt microheater V_h . Dotted line is a quadratic fit to the plots. Monotonic increase in ΔV_p with V_h^2 suggests heating of the contact via the Joule heat occurring at the biased Pt coil. (c), Average ΔV , ΔV_{ave} , plotted against the corrected junction conductance $G_c = 1/(1/G - R_s)$ with the serial resistance $R_s = 800 \Omega$. Solid lines are Gaussian fits to the distribution with dotted lines indicating their center positions, $G_{m,i}$ ($i = 1, 2, 3$). The oscillation of ΔV_{ave} at above $1 G_0$ is in close agreement with the quantized thermoelectric power expected in a ballistic one dimensional system. Color coding denotes peaks positioned at $G_{m,i}$: black = $G_{m,1}$, blue = $G_{m,2}$, and green = $G_{m,3}$. (d), $G_{m,i}$ obtained in a range of V_h from 2.0 V to 3.0 V. Dotted lines show the average values. (e), Standard deviation Q of ΔV plotted against G_c . Dotted lines denote the conductance $G_{SD,i}$ whereat Q shows local maxima. Blue line is the theoretical Q derived from the coherent backscattering model. (f), Plots of the peak positions $G_{SD,i}$ extracted from (e). Dotted lines are at the average conductance.



$\Delta V_{ave} = \sum_i^n \Delta V_i / N$ together with the standard deviations $Q = [\sum_i^n (\Delta V_i - \Delta V_{ave})^2 / N]^{0.5}$ and plotted with respect to the junction conductance (Figs. 2c–f), where N is the number of thermoelectric voltage data ΔV_i within a conductance window of $0.02 G_0$. Interestingly, whereas ΔV_{ave} is almost constant in a high conductance regime, several peaks are detected at $G_{m,i}$ below $3 G_0$ (note that the influence of the series resistance $R_s = 800 \Omega$ is subtracted from G as $G_c = 1/(1/G - R_s)$ in Fig. 2c). We find that these characteristic peaks emerge at a well-defined conductance of $G_{m,1} = 0.70 G_0$, $G_{m,2} = 1.54 G_0$, and $G_{m,3} = 2.30 G_0$ irrespective of V_h (Fig. 2d; see also Figs. S7 and S8). This fairly agrees with thermopower oscillations expected to take place in the quantum regime of a ballistic conductor that anticipates ΔV maxima at $(n + 0.5 G_0)$ [$n = 1, 2, 3, \dots$]^{23,24}.

The quantum nature of electron transport in atomic junctions is also identified in the thermo-voltage fluctuations. $Q - G$ plots at $V_h = 2.0$ V reveal strong suppression of the thermoelectric voltage fluctuations at nG_0 (Fig. 2e; G is corrected by $R_s = 800 \Omega$ similar to the case in Fig. 2c). This characteristic property is reproduced in the V_h range measured (Fig. 2f). Theoretically, fluctuations of thermopower stemming from coherent electron backscattering in vicinity of the contact scales with $\left\{ \sum_i^n T_i^2 (1 - T_i) \right\}^{0.5} / \sum_i^n T_i$, which in fact predicts Q minima when T_i of all the contributing channels is either 0 or 1^{14,25}, and therefore agrees with the transmission-dependent suppression of noise in the thermoelectric voltage observed here. More quantitatively, we extracted up to two peak positions in the $Q - G$ plots, $G_{SD,i}$ ($i = 1, 2$), and plotted against V_h (Fig. 2e). The average values are $G_{SD,1} = 1.59 \pm 0.18 G_0$ and $G_{SD,2} = 2.41 \pm 0.30 G_0$. Meanwhile, the backscattering model⁴ yields local Q maxima at $1.56 G_0$ and $2.61 G_0$, which are in accordance with the experimental $G_{SD,i}$ within 2% and 8% error for $G_{SD,1}$ and $G_{SD,2}$, respectively.

The above results indicate predominant roles of quantum confinement effects on the thermoelectric transport in ballistic atom-sized contacts. We demonstrate herein that the conductance-dependent thermoelectric power also provides insight into the geometry-sensitive electronic structures of Au single-atom chains. As depicted in Fig. 2c, ΔV tends to show a deep minimum at one unit of the conductance quantum and attains a positive maximum at around $0.6 G_0$. This can be interpreted qualitatively as arising from weakening of contact-lead coupling in single-atom chains under elongation^{26,27}. In an unstrained fully transparent single-atom contact, s -electrons are delocalized along the chains and the peak of a broad transmission curve is located at the Fermi level E_F (Fig. 3b)²⁶. Under this condition, the thermoelectric power is very small (Regime I)^{9,13}. In contrast, the coupling is weakened as Au-Au bonds are stretched that contributes to shift and narrow the transmission curve²⁶. In a weak coupling case, S_c is defined as $S_c = (\pi^2 k_B^2 T_c / 3e) (\partial \ln T_i / \partial E|_{E=E_F})$ ²⁸, which increases rapidly as moving slightly away from the resonance condition (Regime II). On the other hand, further straining leads to concomitant decrease in G and S_c (Regime III)^{26,28}.

Interestingly, the thermoelectric power of single-atom contacts in many cases changed from positive to negative (Fig. 3c–d). Depending on the contact mechanics, in conjunction with a possible influence of gas molecule adsorptions²⁹, a single-atom contact evolves into various motif with different transmission lineshapes^{26,30}. Sign inversion can take place when a transmission valley crosses over the Fermi level (Fig. 3e), where at the same time thermoelectric voltage would become much sensitive to a change in the electronic structure giving rise to large fluctuations in ΔV (Fig. 2e). The negative ΔV_{ave} thus indicates formations of atomic chains with a local minimum of transmission at near the Fermi level (Fig. 3e)²⁶.

Particular interest lies in estimating thermopower of single-atom contacts from the ΔV measurements; a prerequisite for evaluation of the thermoelectric performance. It requires analyses of the actual

temperature gradient ΔT_c at the junction. For this, we utilized the lifetime τ of single-atom contacts as atomic thermometer described as $\tau = f_0^{-1} \exp(-E_B/k_B T_c)$ ^{31,32}. Here, $f_0 = 3 \times 10^{12}$ Hz, E_B , k_B , and T_c denote the attempt frequency, the critical bond strength in the contact, Boltzmann factor, and the effective temperature at a breakpoint in the atomic wires. The average lifetime τ_{ave} acquired from 1 G_0 plateau lengths (Fig. 4a, inset; see also Fig. S9) decayed exponentially with V_h (Fig. 4a) suggesting steady increase in T_c with V_h ³³. Extrapolation of the $\log(\tau_{ave}) - V_h$ dependence to $V_h = 0$ V gives $E_B = 0.82$ eV, typical for Au single-atom contacts. We back-calculated T_c from τ_{ave} using the energy barrier height (Fig. 4b). As it is clear from Figs. 2b and S6 that the contact heats up with V_h ², due to the fact that the Joule heat at the heater carrying current I increases with the power $IV_h = V_h^2/R$, where R is the resistance of the Pt coil, we fit the $T_c - V_h$ plots as a function of V_h^2 to deduce the local temperature gradient formed at the Au single-atom wire ΔT_c (the cold side is assumed to be remained at the ambient temperature⁷). The relatively low T_c compared to the local temperature at the microheater under elevated V_h (Fig. S6) is ascribed to heat leakage through the Au lead and Al_2O_3 layer. The thermopower of the Au single-atom chain S_c is deduced from ΔV_c , which is the maximal positive ΔV at $G < 1 G_0$. Noticeably, we find that ΔV_c rises linearly with ΔT_c at low ΔT_c and tends to increase faster at $\Delta T_c > 15$ K (Fig. 4c). Accordingly, the acquired S_c obtained through $S_c = S_{Au} - \Delta V_c / \Delta T_c$ (Fig. S10) is around $-4 \mu V/K$ at low ΔT_c whereas it decreases to -6 to $-8 \mu V/K$ under larger ΔT_c .

Discussion

The present results indicate that what largely determines the thermopower of Au atom-sized contacts is the geometry at their bank region that gives rise to both positive and negative ΔV irrespective of the conductance (Fig. S5). This geometrical dependence, which is characterized as a random noise due to the stochastic nature of the mechanical deformation processes during contact elongation, can be smoothed by data averaging, by which the intrinsic quantum properties of atom-sized junctions, such as the conductance-dependent thermopower oscillation, becomes observable. Here, it is noticeable that the experiment performed by Ludoph and van Ruitenbeek¹⁴ in a cryogenic vacuum failed to detect the oscillation behavior in Au nanocontacts ascribed to the considerable fluctuation in the thermopower data¹⁴. The discrepancy stems presumably from the fact that we finely controlled the contact mechanics via a feedback mechanism to hinder fusing of the contact during the formation processes (the junction conductance was below $15 G_0$ throughout the experiments), which enabled to make the structure of the electrodes in the bank relatively intact leading to diminished thermopower fluctuations derived from the electron backscattering. On the other hand, such procedure was not incorporated in the previous work¹⁴ implying a large structural variation in the bulk electrodes involved in the break-junction measurement. This manifests the importance of having special care to preserve the geometry of bulk regions in order to evaluate the quantum effects on the thermoelectric properties of nanocontacts.

The negative sign of the Seebeck coefficient of Au nanocontacts found here is in agreement with theory that predicts thermopower quantization at $S_c = k_B \ln 2 / e (n + 1/2) \sim -60 / (n + 1/2) \mu V/K$ for the n th sub-band in a ballistic one-dimensional system^{23,34}, where k_B and e are the Boltzmann constant and the electron charge, respectively. Moreover, as shown in Fig. 4c, S_c obtained at $G_{m,2}$ is larger than that at $G_{m,3}$. This can also be explained by the theoretical model that anticipates smaller thermoelectric power at higher sub-band states. Quantitatively, however, the theoretical thermopower for $n = 1$ should be a factor of 1.7 higher than that at $n = 2$, whereas the ratio of the experimental S_c at $G_{m,2}$ and $G_{m,3}$, which should correspond to the first and the second sub-band states, is approximately 1.4. In addition, the measured Seebeck coefficients are an order of

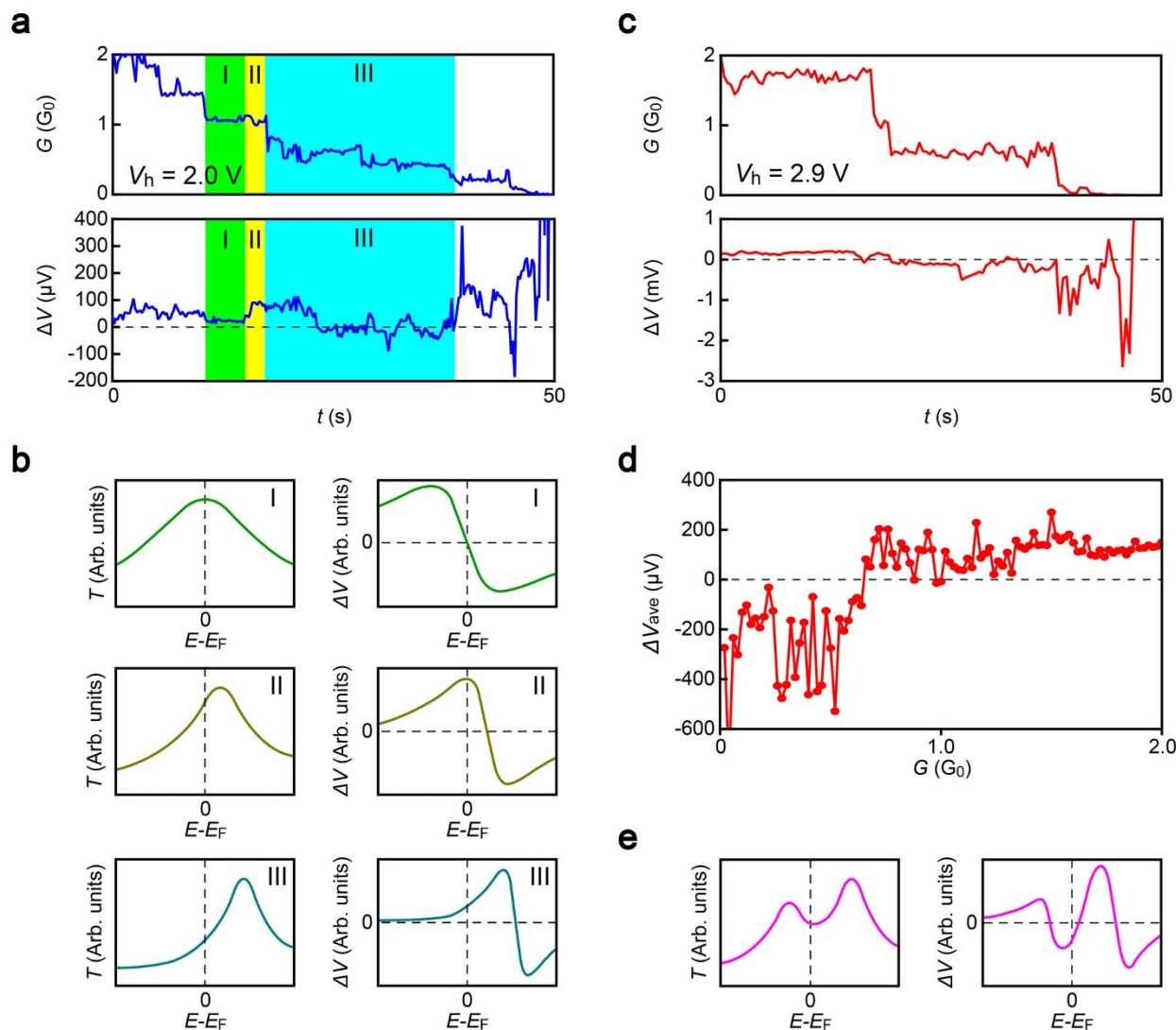


Figure 3 | Geometry-sensitive thermoelectric voltage of single-atom contacts. (a), G and ΔV traces at $V_h = 2.0$ V and (b), the corresponding transmission curves deduced for different stages of contact stretching. The transmission peak is at around the electrode Fermi level E_F when G is close to $1 G_0$. At this point, ΔV is very small (Region I). Pulling the junction, a single-atom chain is elongated that weakens contact-lead coupling and shifts the narrowed transmission curve. Whereas the single-atom conductance tends to be zero in a stepwise manner, this first gives rise to a rapid increase (Region II) followed by monotonic decrease in ΔV (Region III). (c–d), Sign inversion of thermoelectric voltage in single-atom contacts. Negative ΔV was found occasionally at below $1 G_0$. A transition occurs at G_T . (e), The positive-to-negative transition of the thermoelectric voltage is ascribable to the existence of a local minimum in the transmission curve near E_F .

magnitude smaller than the theoretical value. These discrepancies presumably stem from the assumption that the local temperature at one side of the contact remains at the ambient even under high V_h conditions that may not be applicable for Au atom-sized contacts considering the high thermal conductivity of gold: unlike molecular junctions¹³, thermal transport through the heat-conductive metallic nanocontact would make the actual temperature gradient smaller than ΔT_c , which leads to underestimation of S_c .

Methods

Fabrication of heater-embedded MCBJs. Heater-embedded MCBJs are fabricated as follows. We first formed a 4 μ m-thick polyimide layer on a mirror-polished surface of a 0.5 mm-thick phosphor bronze substrate by spin-coating and baking on a hot plate. We then rendered a microelectrode pattern by a photolithography method using a photoresist AZ-5206E. Subsequently, a Au/Cr multilayer of thickness 25 nm/5 nm was deposited by a radio-frequency magnetron sputtering. The substrate was then immersed in N, N-dimethylformamide (DMF) for more than 8 hours and ultrasonicated for lift off. After that, we delineated an Al_2O_3 thin film pattern by an electron-beam lithography method using a resist ZEP-520A-7. Al_2O_3 of 25 nm thickness was then deposited using the sputtering method followed by a lift-off in DMF. On the Al_2O_3 , a heater pattern is drawn by the EB lithography. By depositing

40 nm thick Pt by the sputtering and removing the resist in DMF, we obtained Pt nanowire of 350 nm width. Following this, we further fabricated a 100 nm thick Au nanowire with a narrow constriction of 100 nm width at the middle using the same lithography and sputtering processes. The sample was then exposed to isotropic reactive ion etching (50 W, O_2) to remove the polyimide underneath the Au nanowire. As a result, we obtained a Au nanobridge of length about 2 μ m. This geometry provides the attenuation factor r of 3×10^{-4} ¹⁷, which enables fine-control of the tensile displacements on the junction at sub-picometer level.

Formation of gold single-atom contacts. We formed Au single-atom contacts using a self-breaking technique. Specifically, we mounted a heater-integrated MCBJ on a stage in a three-point bending configuration and evacuated the sample chamber to below 10^{-5} Torr. The MCBJ substrate was then bended mechanically from the back using a piezo-driven pushing rod at room temperatures. Meanwhile, the electrical conductance G of the junction was monitored at a bias voltage V_b of 0.1 V. Here, the conductance was used as a reference to control the stretching speed v_d of the junction: v_d was kept at 6 nm/s at $G > 10 G_0$ until G decreases to $10 G_0$ where the stretching rate is lowered to 0.6 nm/s and finally to $v_d = 0.0006$ nm/s when it fell below $5 G_0$. After breakdown, we moved the piezo-element in the opposite direction and formed a contact. During the formation process, a special care was taken to make conductance not to exceed $15 G_0$ so as to prevent fusing of the contact. This conductance feedback control of contact mechanics allowed forming and holding single-atom contacts for prolonged time necessary for conducting the thermoelectric voltage measurements³³.

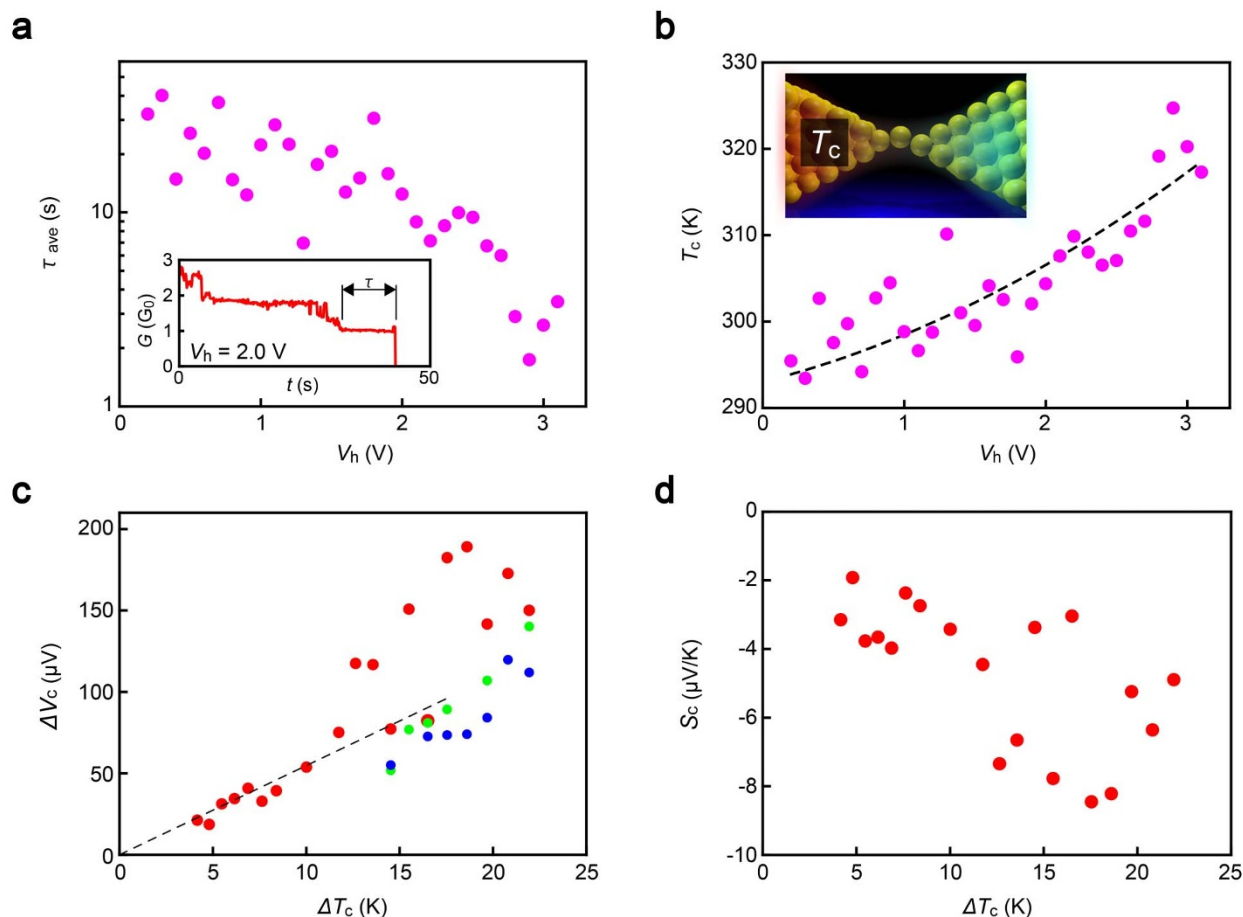


Figure 4 | Thermopower of Au single-atom contacts. (a), The average holding time τ of single-atom contacts (inset) that demonstrates exponential decay with V_h . (b), The effective temperature T_c at the hot side of single-atom chains obtained from (a). Broken line is a quadratic fit to the plot. (c), Thermovoltage of single-atom contacts ΔV_c obtained from the peak at $G_{m,1}$ (red), $G_{m,2}$ (green), and $G_{m,3}$ (blue) plotted against the local temperature gradient ΔT_c . Dotted line is a linear fit at $\Delta T_c < 15$ K. (d), Thermopower S_c of single-atom contacts.

Thermoelectric voltage and electrical conductance measurements. Simultaneous measurements of the thermoelectric voltage and the electrical conductance were performed when G decreases below $8 G_0$ during the feedback controlled stretching of Au nanocontacts. For this, a dc voltage V_h was applied to the Pt microheater by a picoammeter-source unit (Keithley model 6487) to impose a temperature gradient on the junction via heat conduction through the Al_2O_3 layer. The picoammeter was also exploited for calibration of the Pt microheater (Fig. S6). Note that the polyimide layer is used not only for electrical insulation but also as a thermal insulator for impeding heat leakage through the substrate. In the break junction measurements, G was measured under a voltage of $V_b = 0.1$ V using another ammeter (Keithley model 6487). A protection resistance of 10 k Ω was connected to prevent from overcurrent breakdown of fused junctions. After each conductance measurement, voltage across the junction was recorded using a nanovoltmeter (Keithley model 2182) with voltage source being switched off. The sampling rate of the simultaneous recording was approximately 3 Hz.

Pt microheater calibration. In prior to the break junction experiments, we carried out a calibration of the Pt heater (Fig. S6). We controlled the temperature of the sample stage T_0 using a resistive heater and a thermometer attached to it using a temperature controller (Scientific Instruments model 9700). The resistance of the microheater R_{Pt} was then recorded using a picoammeter-source (Keithley model 6487) at various T_0 above room temperatures. After that, $R_{Pt} - V_h$ characteristics were measured by the same ammeter. The thus quantitated $R_{Pt} - T_0$ relationship was used as a calibration curve to deduce the local temperature at the microheater under elevated V_h conditions during the thermoelectric voltage measurements.

Data analysis. Background in the thermoelectric voltage measurements was calibrated by measuring the $V_m - G$ dependence with no heat added and subtracting it from the data at $V_h > 0$ V. After that, the thermoelectric voltage ΔV was deduced as $\Delta V = V_m(1 + 12900/G/R_p)$, where G and R_p are the junction conductance in G_0 unit and the resistance of the 10 k Ω protective resistor. ΔV_{ave} and Q were calculated from ΔV data binned at 0.01 G_0 , which were obtained in the consecutive 50 junction

opening/closing processes. ΔV_c were extracted by Gaussian fitting to the ΔV_{ave} in the positive regime within a conductance window of 0 to 1 G_0 .

1. Zebarjadi, M., Esfarjani, K., Dresselhaus, M. S., Ren, Z. F. & Gang, C. Prospectives on thermoelectrics: From fundamentals to device applications. *Energy Environ. Sci.* **5**, 5147–5162 (2012).
2. Sootsman, J. R., Chung, D. Y. & Kanatzidis, M. G. New and old concepts in thermoelectric materials. *Angew. Chem. Int. Ed.* **48**, 8616–8639 (2009).
3. Li, J.-F., Liu, W.-S., Zhao, L.-D. & Zhou, M. High-performance nanostructured thermoelectric materials. *NPG Asia Mat.* **2**, 152–158 (2010).
4. Snyder, G. J. & Toberer, E. S. Complex thermoelectric materials. *Nat. Mat.* **7**, 105–114 (2008).
5. Hicks, L. D. & Dresselhaus, M. S. Thermoelectric figure of merit of a one-dimensional conductor. *Phys. Rev.* **47**, 16631–16634 (1993).
6. Vineis, C. J., Shakouri, A., Majumdar, A. & Kanatzidis, M. G. Nanostructured thermoelectrics: Big efficiency gains from small features. *Adv. Mat.* **22**, 3970–3980 (2010).
7. Reddy, P., Jang, S.-Y., Segalman, R. A. & Majumdar, A. Thermoelectricity in molecular junctions. *Science* **315**, 1568–1571 (2007).
8. Malen, J. A., Yee, S. K., Majumdar, A. & Segalman, R. A. Fundamentals of energy transport, energy conversion, and thermal properties in organic-inorganic heterojunctions. *Chem. Phys. Lett.* **491**, 109–122 (2010).
9. Dubi, Y. & Di Ventra, M. Colloquium: Heat flow and thermoelectricity in atomic and molecular junctions. *Rev. Mod. Phys.* **83**, 131–155 (2011).
10. Shapira, E., Holtzman, A., Marchak, D. & Selzer, Y. Very high thermopower of Bi nanowires with embedded quantum point contacts. *Nano Lett.* **12**, 808–812 (2012).
11. Widawsky, J. R., Darancet, P., Neaton, J. B. & Venkataraman, L. Simultaneous determination of conductance and thermopower of single molecule junctions. *Nano Lett.* **12**, 354–358 (2011).
12. Malen, J. A., Doak, P., Baheti, K., Majumdar, A. & Segalman, R. A. The nature of transport variations in molecular heterojunction electronics. *Nano Lett.* **9**, 3406–3412 (2011).



13. Dubi, Y. & Di Ventra, M. Thermoelectric effects in nanoscale junctions. *Nano Lett.* **9**, 97–101 (2011).
14. Ludoph, B. & van Ruitenbeek, J. M. Thermopower of atomic-size metallic contacts. *Phys. Rev. B* **59**, 12290–12293 (1999).
15. Kim, P., Shi, L., Majumdar, A. & McEuen, P. L. Thermal transport measurements of individual multiwalled nanotubes. *Phys. Rev. Lett.* **87**, 215502 (2001).
16. van Ruitenbeek, J. M. *et al.* Adjustable nanofabricated atomic size contacts. *Rev. Sci. Instrum.* **67**, 108–111 (1996).
17. Agraït, N., Yeyati, A. L. & van Ruitenbeek, J. M. Quantum properties of atomic-sized conductors. *Phys. Rep.* **377**, 81–279 (2003).
18. Landauer, R. Electrical resistance of disordered one-dimensional lattices. *Phil. Mag.* **21**, 863–867 (1970).
19. Krans, J. M., van Ruitenbeek, J. M., Fisum, V. V., Yanson, I. K. & de Jongh, L. J. The signature of conductance quantization in metallic point contacts. *Nature* **375**, 767–769 (1995).
20. van Wees, B. J. *et al.* Quantised conductance of point contacts in a two-dimensional electron gas. *Phys. Rev. Lett.* **60**, 848–850 (1988).
21. Thijssen, W. H. A., Marjenburgh, D., Bremmer, R. H. & van Ruitenbeek, J. M. Oxygen-enhanced atomic chain formation. *Phys. Rev. Lett.* **96**, 026806 (2006).
22. Csonka, Sz. *et al.* Fractional conductance in hydrogen-embedded gold nanowires. *Phys. Rev. Lett.* **90**, 116803 (2003).
23. van Houten, H., Molenkamp, L. W., Beenakker, C. W. J. & Foxon, C. T. Thermoelectric properties of quantum point contacts. *Semicond. Sci. Technol.* **7**, B215–B221 (1992).
24. Dzurak, A. S. *et al.* Thermopower of a one-dimensional ballistic constriction in the non-linear regime. *J. Phys.: Cond. Matter* **5**, 8055–8064 (1993).
25. Pauly, F. *et al.* Molecular dynamics study of the thermopower of Ag, Au, and Pt nanocontacts. *Phys. Rev. B* **84**, 195420 (2011).
26. Grigoriev, A. *et al.* Electron transport in stretched monoatomic gold wires. *Phys. Rev. Lett.* **97**, 236807 (2006).
27. Kizuka, T. Atomic configuration and mechanical and electrical properties of stable gold wires of single-atom width. *Phys. Rev. B* **77**, 155401 (2008).
28. Paulsson, M. & Datta, S. Thermoelectric effect in molecular electronics. *Phys. Rev. B* **67**, 241403 (2003).
29. Sciauzero, G., Corso, A. D. & Smogunov, A. Effect of stretching on the ballistic conductance of Au nanocontacts in presence of CO: A density functional theory. *Phys. Rev. B* **85**, 165412 (2012).
30. Jelínek, P., Pérez, R., Ortega, J. & Flores, F. *Ab initio* study of evolution of mechanical and transport properties of clean and contaminated Au nanowires along the deformation path. *Phys. Rev. B* **77**, 115447 (2008).
31. Todorov, T. N., Hoekstra, J. & Sutton, A. P. Current-induced embrittlement of atomic wires. *Phys. Rev. Lett.* **86**, 3606–3609 (2001).
32. Tsutsui, M., Taniguchi, M. & Kawai, T. Local heating in metal-molecule-metal junctions. *Nano Lett.* **8**, 3293–3297 (2008).
33. Tsutsui, M. *et al.* Atomically controlled fabrications of subnanometer scale electrode gaps. *J. Appl. Phys.* **108**, 064312 (2010).
34. Streda, P. Quantised thermopower of a channel in the ballistic regime. *J. Phys.: Condens. Matter.* **1**, 1025–1027 (1989).

Acknowledgments

This research was supported in part by Strategic Information and Communications R&D Promotion Programme (122107001) of Ministry of Internal Affairs and Communications and “Nanotechnology Platform Project (Nanotechnology Open Facilities in Osaka University)” of Ministry of Education, Culture, Sports, Science and Technology, Japan [No: F-12-OS-0016]. M. Tsutsui acknowledges support from Foundation Advanced Technology Institute, The Thermal & Electric Energy Technology Foundation, Kansai Research Foundation for technology promotion, and Yazaki Memorial Foundation for Science and Technology.

Author contributions

M.T. and M.T. planned and designed experiments. M.T. and T.M. fabricated microheater-embedded MCBJs and conducted break junction measurements. M.T., T.M. and A.A. performed data analyses. M.T. and M.T. co-wrote paper.

Additional information

Supplementary information accompanies this paper at <http://www.nature.com/scientificreports>

Competing financial interests: The authors declare no competing financial interests.

How to cite this article: Tsutsui, M., Morikawa, T., Arima, A. & Taniguchi, M. Thermoelectricity in atom-sized junctions at room temperatures. *Sci. Rep.* **3**, 3326; DOI:10.1038/srep03326 (2013).



This work is licensed under a Creative Commons Attribution-NonCommercial-ShareAlike 3.0 Unported license. To view a copy of this license, visit <http://creativecommons.org/licenses/by-nc-sa/3.0>